

## Article

# Reinforcement of Aminopropyl-Terminated Siloxane-Treated Carbon Nanotubes in Epoxy Thermosets: Mechanical and Thermal Properties

Yuxin Sun <sup>1,2</sup>, Xiwen Zhang <sup>1,2</sup> and Dongyu Zhao <sup>1,2,\*</sup>,<sup>†</sup>

<sup>1</sup> School of Chemistry and Materials Science, Heilongjiang University, Harbin 150080, China; sunyuxin\_xl@163.com (Y.S.); zwxrun@163.com (X.Z.)

<sup>2</sup> Key Laboratory of Chemical Engineering Process & Technology for High-Efficiency Conversion, College of Heilongjiang Province, Harbin 150080, China

\* Correspondence: zhaodyu@hlju.edu.cn

<sup>†</sup> Current address: College of Chemical Engineering and Materials, Heilongjiang University, Xuefu Street 74#, Harbin 150080, China.

**Abstract:** The synthesis and characterization of aminopropyl-terminated polydimethylsiloxane-treated carbon nanotube (AFCNT)-reinforced epoxy nanocomposites are reported in the current study. The amine functionalization of the CNTs was performed with a reaction to PDMS-NH<sub>2</sub>. The AFCNTs were homogeneously dispersed in epoxy resin by using an emulsifier and a three-roller mill. The AFCNTs were characterized using Fourier-transform infrared spectroscopy (FTIR) and scanning electron microscopy (SEM). The curing behavior of the epoxy/AFCNT was studied using a differential scanning calorimeter (DSC). The tensile and impact strengths of the 2.0 wt.% AFCNT-reinforced epoxy nanocomposite were enhanced by 43.2% and 370%, respectively. Moreover, the glass transition temperature ( $T_g$ ) was also enhanced by 21 °C. Furthermore, significant enhancements were observed in the initial degradation and char yield values. SEM results confirmed that the AFCNTs were highly dispersed in the polymeric matrix.

**Keywords:** amine functionalization; carbon nanotubes; nanocomposites; mechanical properties



**Citation:** Sun, Y.; Zhang, X.; Zhao, D.

Reinforcement of Aminopropyl-Terminated Siloxane-Treated Carbon Nanotubes in Epoxy Thermosets: Mechanical and Thermal Properties. *Polymers* **2023**, *15*, 3184. <https://doi.org/10.3390/polym15153184>

Academic Editor: Angels Serra

Received: 8 July 2023

Revised: 24 July 2023

Accepted: 25 July 2023

Published: 27 July 2023



**Copyright:** © 2023 by the authors. Licensee MDPI, Basel, Switzerland. This article is an open access article distributed under the terms and conditions of the Creative Commons Attribution (CC BY) license (<https://creativecommons.org/licenses/by/4.0/>).

## 1. Introduction

The invention and application of epoxy resins have brought great convenience to people's lives [1]. Epoxy resins are widely used in industry for various applications, such as adhesives [2–4], coatings [5,6], packaging [7,8], and other structural materials [9–11]. The epoxy resins have a higher degree of crosslinks, thus showing thermosetting properties; for instance, higher degrees of rigidity and better strength and dimensional stability. However, the shortcomings of epoxy resin, such as its poor heat resistance and brittleness, has gradually begun to have an impact on its range of applications in the industry [12].

The carbon nanotube (CNT), a one-dimensional linear allotrope of carbon having a higher surface area, has attracted exceptional attention since its discovery, due to its outstanding mechanical and thermal properties [13,14]. Numerous studies have been done to improve its mechanical and thermal properties by reinforcing this promising nanomaterial in the field of polymer composites [15–17]. However, the blending of the CNT in the polymeric matrix is quite difficult due to the existence of its own strong van der Waals force and the formation of a very serious self-agglomeration. Various physical dispersion and chemical modification methods have been used to prevent the agglomeration of CNTs [18,19]. These methods include functionalization by covalent methods, non-covalent methods, polymers, and biomolecules and decoration with nanoparticles and surfactants [20]. Researchers reported that the dispersion and synergy of CNTs can be improved within the matrix resin by surface functionalization [21]. It has been demonstrated

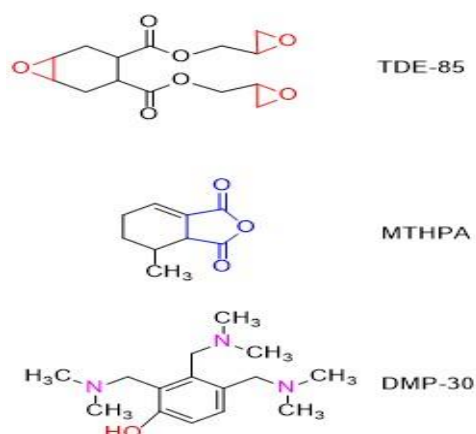
that functionalized CNTs as effective reinforcing fillers offer the possibility to achieve a good balance between high thermal stability and excellent mechanical properties of epoxy composites [20,22]. The CNT's surface was chemically modified with vitamin B2 under microwave irradiation and reinforced in biodegradable poly(ester-imide) by Mallakpour and Soltanian [23]. Similarly, in another study by Mallakpour and Zadehnazari, CNTs were acid-modified and provided reinforcement in poly(amide-imide) [24]. Moreover, CNTs were functionalized with poly-L-lysine by a non-covalent method with N-carboxy anhydride polymerization by Ling and coworkers [25]. Donchak and coworkers observed that  $\text{NH}_2$ -modified CNTs can be easily dispersed in a thermoplastic matrix [26]. In addition to this, the mechanical properties of the produced nanocomposites with  $\text{NH}_2$ -modified CNTs were much better than those with non-modified CNTs containing nanocomposites. Based on these works, improvement of the properties of CNT polymer matrix composites largely depends on the good compatibility between the CNT and polymer matrix. The better the compatibility, the higher the dispersion and the more obvious the macroscopic performance change. Therefore, it is crucial to solve the agglomeration problem of CNTs and improve their dispersion in the polymer matrix.

In the present work, we proposed a new method to deal with the process complexity and irreversible agglomeration caused by the presence of varying degrees of drying. The CNTs were functionalized by using aminopropyl-terminated polydimethylsiloxane. Later, the epoxy matrix and treated CNTs were uniformly mixed by using an organic solvent. The mixture was dried and milled to achieve a uniform dispersion of the CNTs in the matrix. The mechanical properties and heat resistance of the nanocomposites were systematically studied.

## 2. Experiment

### 2.1. Materials

A 4,5-epoxycyclohexane-1,2-dicarboxylic acid diglycidyl ester (TDE-85) epoxy matrix was supplied by Tianjin Jingdong Chemical Composites Co., Ltd. (Tianjin, China). Methyltetrahydrophthalic anhydride (MTHPA) and 2,4,6-tris(dimethylaminomethyl) phenol (DMP-30) were purchased from Zhejiang Alpha Chemical Technology Co., Ltd. (Zhejiang, China). CNT with a 20–40 nm diameter and about 5–15  $\mu\text{m}$  length was purchased from Shenzhen Nanotech Port Co., Ltd., (Shenzhen, China). Aminopropyl-terminated polydimethylsiloxane (PDMS- $\text{NH}_2$ ) was purchased from Zhengzhou Alfa Chemical Co., Ltd. (Zhengzhou, China). Sulphuric acid ( $\text{H}_2\text{SO}_4$ ) and nitric acid ( $\text{HNO}_3$ ) were supplied by Tianjin Kemiou Chemical Reagent Co., Ltd. (Tianjin, China).  $N,N'$ -dicyclohexylcarbodiimide (DCC) was supplied by Shanghai Aladdin Chemical Reagent Co., Ltd. (Shanghai, China). Ethanol, acetone, and  $N,N'$ -dimethylformamide (DMF) were purchased from Tianjin City Fu Yu Fine Chemical Co., Ltd. (Tianjin, China). The chemical structures of the resin, hardener, and accelerator are shown in Scheme 1.



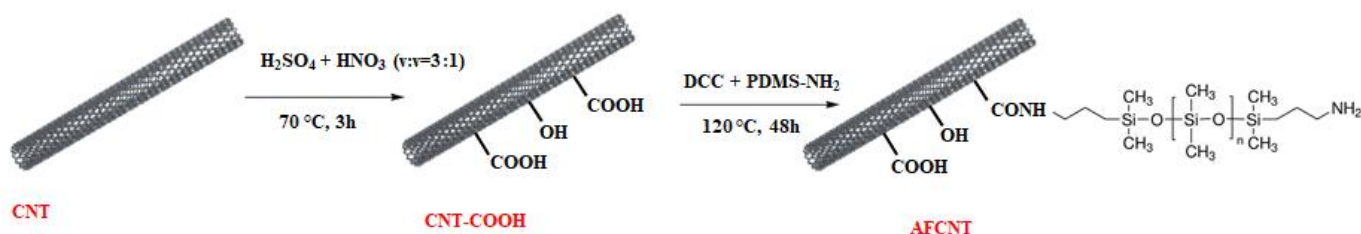
**Scheme 1.** Chemical structures of resin, hardener, and accelerator used in the study.

## 2.2. Synthesis of CNT-COOH

CNTs were treated with an  $\text{H}_2\text{SO}_4$  and  $\text{HNO}_3$  mixed acid solution with a volume ratio of 3:1. The reactants were mechanically stirred for 3 h at  $70^\circ\text{C}$  to implant the oxide groups on the CNT surface. The suspension was cooled to room temperature, and washed several times with distilled water until the filtrates' pH value became neutral. The filter cake was transferred to a freeze dryer and dried for 12 h to obtain oxidized carbon nanotubes (CNT-COOH).

## 2.3. Preparation of Amino-Functionalized CNT

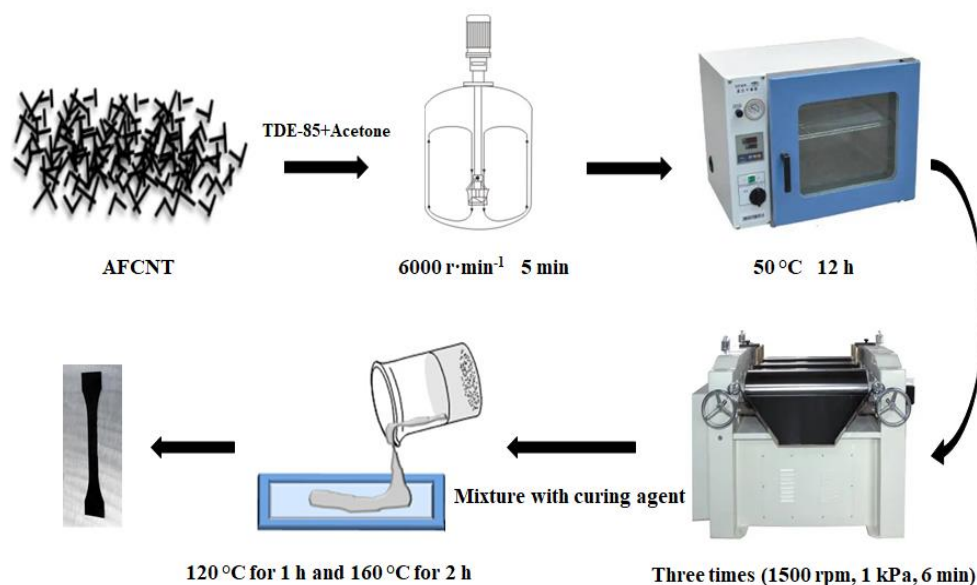
CNT-COOH 0.05 g, PDMS- $\text{NH}_2$  10 mL, DMF 15 mL, and DCC 0.8 g were added into a 250 mL round bottom flask. The refluxing reaction was carried out at  $120^\circ\text{C}$  for 48 h. After that, the excess raw materials and other by-products were washed away by ethanol under ultrasonic oscillation. Amino-functionalized CNT (AFCNT) was prepared from the filter cake by freeze-drying for 8 h and dried for 12 h in a vacuum oven at  $60^\circ\text{C}$ . Scheme 2 shows the various steps involved in the CNT surface activation.



**Scheme 2.** Surface activation mechanism of CNT.

## 2.4. Preparation of the AFCNT/Epoxy Nanocomposites

AFCNT-reinforced epoxy nanocomposites were prepared by blending and grinding with solvent. Appropriate amounts of AFCNT nanofiller and epoxy resin (TDE-85) were weighed and blended using a high-shear emulsifying machine (Shanghai ELE Mechanical and Electrical Equipment Co., Ltd., Shanghai, China) at 6000 RPM for 5 min, and acetone was added as a solvent for better dispersion of the AFCNT in the resin. Later, the solvent was removed from the mixture in a vacuum oven at  $50^\circ\text{C}$  for 12 h. The uniform dispersion of AFCNTs in the resins was confirmed by grinding the AFCNT/resin blend in a three-roller mill three times. The addition of the curing agent with a 1:1 weight ratio of resin to curing agent was made by a THINKY centrifugal mixer (ARV-310, Tokyo, Japan) vacuum mixer (1500 RPM, 1 kPa, 6 min). Finally, the mixture was poured into preheated steel molds and cured at  $120^\circ\text{C}$  for 1 h and  $160^\circ\text{C}$  for 2 h. The reinforcement of AFCNT nanofillers was varied from 0.5 to 2.5 wt.%, with a regular interval of 0.5 wt.%. During the AFCNT blending, the viscosity of the blend was continuously increased and reached the maximum level at 2.5 wt.% AFCNT blending. Therefore, a further increase during the reinforcing phase was not carried out. For the comparative analysis, the neat epoxy resin sample was cured with a similar procedure; however, AFCNT nanofiller was not added. Scheme 3 represents the various steps involved in the manufacturing of nanocomposites.



**Scheme 3.** Schematic illustration for the preparation of AFCNT/epoxy nanocomposites.

### 2.5. Characterization

Fourier-transform infrared (FTIR) spectra analyses were performed at room temperature in the range of  $4000\text{--}400\text{ cm}^{-1}$  by using the transmission mode (BRUKER TENSOR-27).

The fracture surface morphologies of the pristine matrix and epoxy nanocomposites were examined by using scanning electron microscopy (SEM) (JSM-IT300, JEOL, Peabody, MA, USA). The fracture surface samples were placed in liquid nitrogen and sputter-coated with a thin layer of gold to reduce any charge build-up on the surface.

Differential scanning calorimetric (DSC) analysis was recorded on a Q20 of TA Instrument (New Castle, DE, USA) from 20 to 200 °C under an  $\text{N}_2$  atmosphere at a heating rate of  $20\text{ °C}\cdot\text{min}^{-1}$ .

The tensile strength tests of the pristine epoxy matrix and nanocomposites were measured on an Instron 5982 electronic tensile machine at room temperature and a rate of  $2\text{ mm}\cdot\text{min}^{-1}$ . Standard dumbbell-shaped specimens ( $100.0\text{ mm} \times 12.5\text{ mm} \times 4.0\text{ mm}$ ) were made by following the ASTM D-638 standard for the tensile test. The impact strength of an  $80\text{ mm} \times 10\text{ mm} \times 4\text{ mm}$  sample size was tested on a PTM 1000 material tester of Shenzhen Sansi Technology Co., Ltd., (Shenzhen, China). For all the mechanical tests, at least five specimens for each single composition were tested.

Thermal stabilities from 50 to 750 °C under an air atmosphere of the neat epoxy matrix and nanocomposites were evaluated on a Q500 Thermo gravimetric analyzer from TA instruments (New Castle, DE, USA) at a  $10\text{ °C}\cdot\text{min}^{-1}$  heating rate.

The glass transition temperature ( $T_g$ ) was estimated from the tan delta peak temperature by studying the thermomechanical properties on a Dynamic Mechanical Analyzer (DMA) Q800, TA instruments (New Castle, DE, USA). Tests were performed in temperatures ranging from room temperature to 250 °C in single cantilever mode at 1 Hz with a constant heating rate of  $5\text{ °C}\cdot\text{min}^{-1}$ .

## 3. Results and Discussion

### 3.1. Characterizations of CNTs

In order to verify the presence of PDMS groups on the top surfaces of functionalized CNTs, a series of FTIR tests were conducted, and the results are shown in Figure 1. In the figure, the three curves represent the CNT, CNT-COOH, and AFCNT samples.

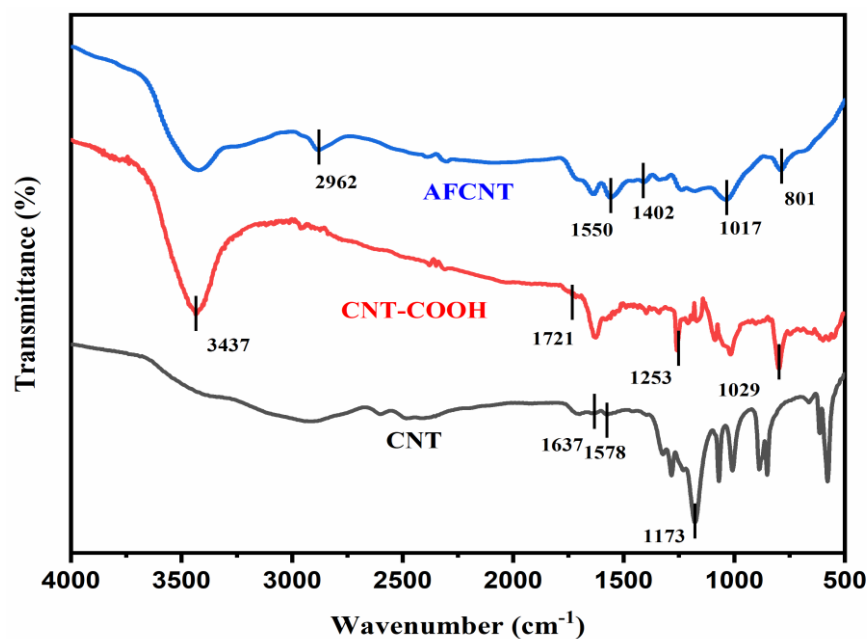


Figure 1. FTIR spectra of pristine, intermediate, and amino-functionalized CNTs.

The CNT sample curve showed three absorption peaks at 1637, 1578, and 1173  $\text{cm}^{-1}$ , respectively. Among them, the absorption peaks at 1637 and 1578  $\text{cm}^{-1}$  were C=C stretching vibration peaks, and the 1173  $\text{cm}^{-1}$  was the stretching vibration absorption peak of C-C, which can be attributed to the C-C stretching vibration of the internal carbon nanotubes.

In the CNT-COOH sample curve, the absorption peaks at 3437 and 1721  $\text{cm}^{-1}$  were the stretching vibration peaks of -OH and C=O, respectively [27]. The absorption peaks at 1253 and 1029  $\text{cm}^{-1}$  can be assigned to the C-O telescopic vibration in the O-CNTs [28,29]. These indicate that oxygen-containing functional groups such as hydroxyl, carboxyl, and others are formed on the CNT surface by oxidation treatment [27].

The AFCNT curve absorption peaks recorded at 2962 and 1017  $\text{cm}^{-1}$  can be easily related to the C-H bonds and Si-O-Si bridge, respectively. The weak symmetric peak at 1402  $\text{cm}^{-1}$  is related to CH<sub>3</sub> [30]. Also, the characteristic peak at 3437  $\text{cm}^{-1}$  was weakened, due to the formation of amide bonds between CNT-COOH and PDMS-NH<sub>2</sub>. The absorption peaks at 1550 and 1402  $\text{cm}^{-1}$  can be assigned to the -NH- bending vibration and the C-N telescopic vibration, respectively. These observations indicate that the CNT-COOH are enriched with oxygen-containing groups after treatment, which facilitates the chemical interactions between CNT-COOH and PDMS-NH<sub>2</sub>.

Substances with a large surface area, such as CNT or graphene, tend to aggregate by themselves, due to the strong van der Waals forces and Coulomb attractions, to form an inevitable lamination, especially during the curing of polymeric resin. SEM images are the most direct means of representing the dispersion of the material. The morphology and microstructure of acidified CNTs (CNT-COOH) and AFCNT were confirmed by SEM, and the obtained morphological images are illustrated in Figure 2.

In Figure 2a, we can easily observe that the acidified CNTs have good dispersion, but also a small degree of inter-tube entanglement, and are ready for the next step, the amino modification of the CNTs. From Figure 2b, it can be seen that the outer layers of AFCNTs after PDMS-NH<sub>2</sub> modification were partially coated with the modified layer, which makes the CNT coarser. This is because the previous acidifying treatment of the CNT made it more end-defective and very easily chemically modified, resulting in PDMS-NH<sub>2</sub> grafting onto CNT.

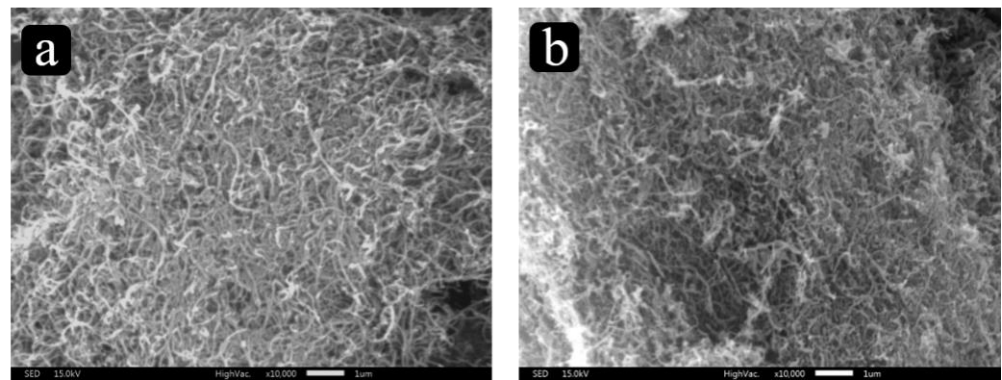


**Figure 2.** SEM micrographs of (a) CNT-COOH and (b) AFCNT.

### 3.2. Curing Behavior of AFCNT/Epoxy Blends

The curing behavior of AFCNT/epoxy blends with different wt.% of AFCNT blending was studied by DSC. The produced DSC curves and data from the AFCNT/epoxy blend are presented in Figure 3 and Table 1, respectively.

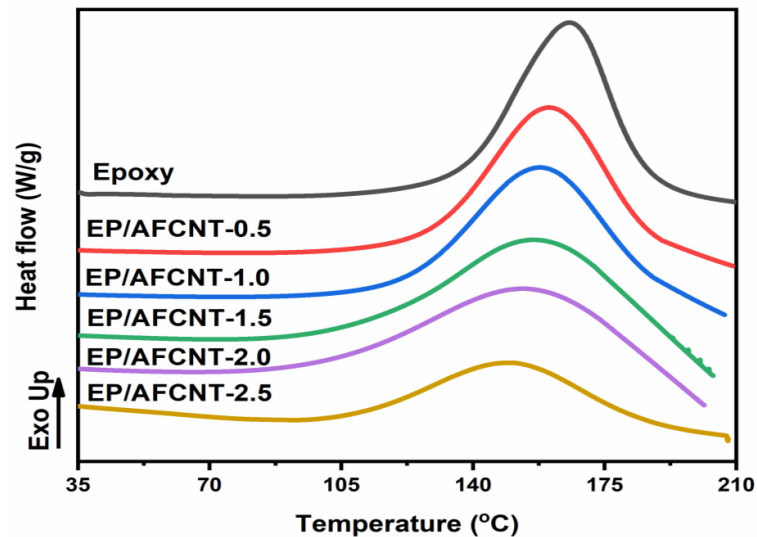


**Figure 3.** DSC spectra of pristine epoxy thermosets and AFCNT/epoxy blends having various AFCNT wt.%.

**Table 1.** DSC parameters of neat epoxy and AFCNT-reinforced nanocomposites.

AFCNT (wt.%)	$T_i$ (°C)	$T_p$ (°C)	$\Delta H$ (J/g)
0	125	165	216.4
0.5	117	160	200.8
1	112	157	187.5
1.5	108	155	184.7
2	103	153	181.7
2.5	98	150	180.6

The produced non-isothermal DSC spectra of pristine epoxy thermosets and AFCNT/epoxy blends having various AFCNT wt.% indicated that the curing peak ( $T_p$ ) gradually weakened and moved towards lower temperatures by increasing the AFCNT blending. This drop in temperature confirms the catalytic effect of  $-NH_2$  groups being attached to AFCNTs [31]. Moreover, the onset curing temperature ( $T_i$ ) was also reduced from 125 to 98 °C as the AFCNT blending was raised. In addition, the curing reaction enthalpy ( $\Delta H$ ) was

gradually decreased from 216.4 to 180.6 J/g as the AFCNT blending was increased from 0 to 2.5 wt.%, respectively. Initially, the decline in  $\Delta H$  was higher, then became slow for >1.0 wt.% blending. This indicates that the higher viscosity of the blends reduces the movement of chain segments and curing reaction [32]. This can be related to the higher energy demand of the epoxy system with the increase in AFCNT blending for the completion of the curing reaction.

### 3.3. Mechanical Properties

The tensile properties and impact intensity of the pure epoxy resin and AFCNT-reinforced epoxy nanocomposites on several AFCNT wt.% reinforcements were studied. Produced tensile strength plots are depicted in Figure 4 and the data extracted from the tensile plots and impact strength values are produced in Table 2.

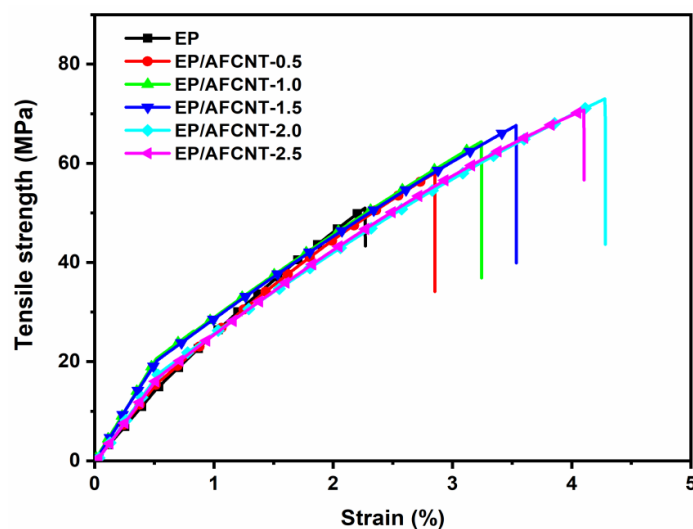


**Figure 4.** Tensile strength–stress curves of the pure epoxy resin and AFCNT-reinforced epoxy nanocomposites.

**Table 2.** Tensile and impact properties of neat epoxy and AFCNT-reinforced nanocomposites.

AFCNT Content (wt.%)	Tensile Strength (MPa)	Tensile Modulus (GPa)	Elongation at Break (%)	Impact Strength ( $\text{kJ}\cdot\text{m}^{-2}$ )
0	$50.98 \pm 3.18$	$3.29 \pm 0.16$	$2.27 \pm 0.21$	$2.86 \pm 0.37$
0.5	$58.05 \pm 2.24$	$3.48 \pm 0.11$	$2.85 \pm 0.18$	$5.67 \pm 0.48$
1	$64.35 \pm 3.87$	$3.66 \pm 0.19$	$3.24 \pm 0.17$	$7.66 \pm 0.73$
1.5	$67.64 \pm 2.69$	$4.00 \pm 0.13$	$3.53 \pm 0.20$	$11.69 \pm 0.38$
2	$73.00 \pm 1.72$	$4.10 \pm 0.17$	$4.28 \pm 0.14$	$12.75 \pm 0.44$
2.5	$70.75 \pm 2.24$	$4.02 \pm 0.11$	$4.10 \pm 0.21$	$13.43 \pm 0.57$

The results showed that with an increase in the AFCNT reinforcement, the tensile strength and modulus values of the nanocomposites first increased and then decreased after attending the optimized loading. A 43.2% improved tensile strength as compared to the recorded value for the pristine matrix was observed with a 2 wt.% AFCNT reinforcement. Tensile strength recorded values for the pristine matrix and optimized-loading (2 wt.%) AFCNT-reinforced epoxy matrix were read as  $50.98 \pm 3.18$  and  $73.00 \pm 1.72$  MPa, respectively. Conversely, loading higher than the optimized amount reduced the tensile strength of nanocomposites to  $70.75 \pm 2.24$  MPa. Meanwhile, with the increase in AFCNTs, the tensile moduli and strain values of the nanocomposites also showed similar behavior.

A similar enhancement in tensile strength was recorded by Mallakpour and Zadehnazari for acid-modified CNT-reinforced poly(amide-imide) that was cured after blending into the matrix by an ultra-sonication-assisted solution process [24]. The tensile strength of

carboxyl-functionalized CNT-reinforced composites was enhanced by 47% upon a 15 wt.% carboxyl-functionalized CNT incorporation. Rahmanian and coworkers reinforced CNT-grown silica in an epoxy thermoset [33]. They reported a 1 wt.% of CNT–silica reinforcement as providing optimized loading, resulting in a 35% higher tensile strength value; moreover, further reinforcement of the CNT–silica showed a decline in enhancement.

The impact intensity of pure epoxy resin and AFCNT-reinforced nanocomposites are also summarized in Table 2. From the data results, we can easily observe that the impact resistance of the AFCNT-reinforced nanocomposites was greatly improved. The impact strength of the nanocomposites was nearly doubled by reinforcing just 0.5 wt.% of AFCNTs in the nanocomposites. After a 1.5 wt.% AFCNT reinforcement, the increase was very slow, as the dispersion was difficult in the resin. However, even a 2.5 wt.% of AFCNT-loaded nanocomposites showed an enhancing trend in the impact strength values. The recorded value ( $13.43 \text{ kJ/m}^2$ ) was 370% higher than the pure epoxy resin value ( $2.86 \pm 0.37 \text{ kJ/m}^2$ ). These enhancements can be attributed to the uniform dispersion of CNTs in the resins, as the reinforced CNTs have better mechanical properties than the pristine matrix [34].

### 3.4. Thermal Properties

The thermal stability of epoxy and AFCNT-reinforced nanocomposites of various AFCNT wt.% in the air atmosphere was studied. Produced spectra are reported in Figure 5 and extracted data from the curves are summarized in Table 3.

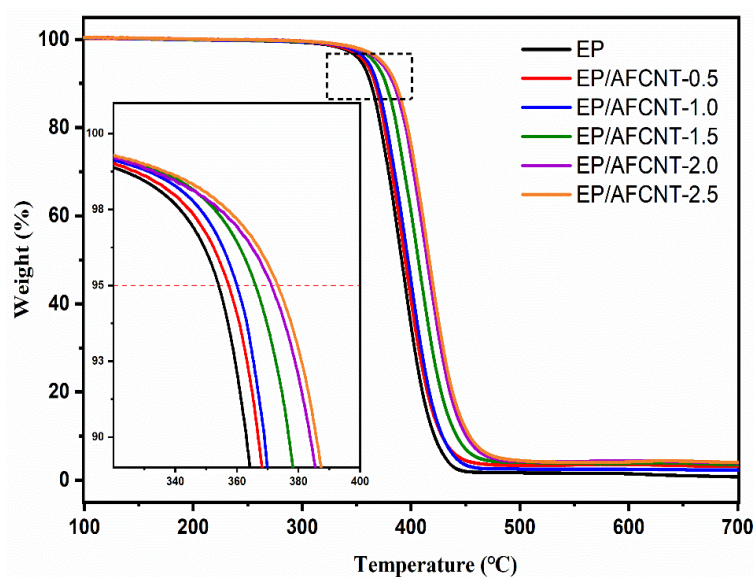


**Figure 5.** TGA curve of neat epoxy and its AFCNT-reinforced nanocomposites.

**Table 3.** TGA parameters of neat epoxy and AFCNT-reinforced nanocomposites.

AFCNT (wt.%)	T <sub>5</sub> (°C)	T <sub>10</sub> (°C)	Y <sub>c</sub> (%) at 700 °C
0	352	363	0.71
0.5	357	367	2.31
1	359	369	3.11
1.5	366	376	3.54
2	371	383	3.94
2.5	374	387	4.06

Epoxy resin has excellent temperature resistance, and is commonly used in packaging materials and high-temperature adhesives [35]. The initial degradation temperatures are those that result 5 and 10 percent weight losses (T<sub>5</sub> and T<sub>10</sub>); for the pristine matrix, these were recorded as 352 and 363 °C. After the reinforcement of the AFCNT nanoparticles in the epoxy matrix, the produced polymeric composites showed improved thermal stabilities;

$T_5$ ,  $T_{10}$ , and char yield at 700 °C ( $Y_c$ ) values were gradually enhanced, and the best values were observed with 2.5 wt.% AFCNT nanoparticle loadings. The recorded values were 22 and 24 °C higher for  $T_5$  and  $T_{10}$ , respectively. Similarly, the  $Y_c$  value was 3.35% higher than the corresponding value for the neat matrix. These enhancements confirm an improved dispersion and interface interaction of the AFCNTs within the matrix. The AFCNT nanocomposites could improve the barrier effect of CNTs and prevent the volatilization of degradation components [16]. This phenomenon has proven the effect of functionalization on the heat resistance of epoxy resin.

### 3.5. The Glass Transition Temperatures of Nanocomposites

The addition of filler can easily affect the glass transition temperatures ( $T_g$ ) of the nanocomposites [36]. The  $T_g$  value can be determined from the  $\tan\delta$  curve produced during DMA analysis. Figure 6 presents the loss factor curve of the pure epoxy resin and AFCNT-reinforced nanocomposites on different AFCNT wt.%.

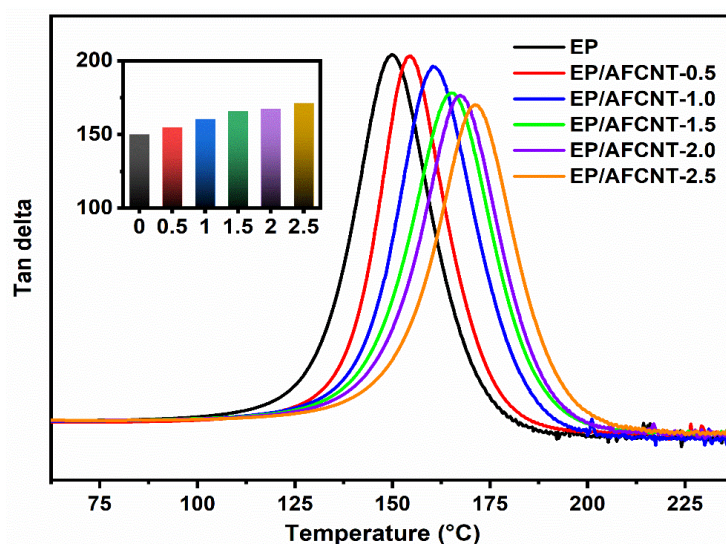


**Figure 6.** Temperature dependence of loss factor ( $\tan\delta$ ) and glass transition temperature for epoxy resin and AFCNT nanocomposites.

As can be observed, with a very low loading of AFCNTs, the  $T_g$  value was significantly increased. The  $T_g$  values for pristine matrix (unfilled) and 2.5 wt.% AFCNT-loaded nanocomposites were recorded as 149.9 and 171.2 °C, respectively. This suggests a cumulative rise of 14.21% in the  $T_g$  value compared to the recorded value for the pure epoxy resin. Moreover, from the  $T_g$  variation pattern produced in the histogram, we can summarize that the amino-functionalized CNT composites can effectively improve heat resistance.

This remarkable enhancement in the  $T_g$  value as compared to the pristine epoxy matrix can be attributed to the AFCNT nanofiller having higher rigidity. Moreover, the  $\tan\delta$  peak height gradually reduced as the loading of the AFCNT nanofiller was raised from 0 to 2.5 wt.% due to the dilution phenomena. In addition to this, the relaxation process was also confirmed for the AFCNT-reinforced epoxy nanocomposites by the broadening of the  $\tan\delta$  peak.

The introduction of an AFCNT fraction in the nanocomposites restricted the molecular chain movement and relatively reduced free volume in the nanocomposites. Specifically, the good compatibility of the AFCNTs with the epoxy results in uniform dispersion of the nanoparticles, which may reduce the mobility of the polymer molecular chains [21]. The interfacial interaction between AFCNTs and the epoxy resin was further enhanced by the ability of the highly reactive group ( $-NH_2$ ) attached to the surface of AFCNT nanocomposites to participate in the epoxy resin curing reaction [37].

### 3.6. Interfacial Interaction Analysis by SEM

The SEM technique is one of the effective ways to evaluate the dispersion of nanofillers in the matrix and interface of nanocomposites. The fracture surface morphology of the nanocomposites observed using SEM is produced in Figure 7.

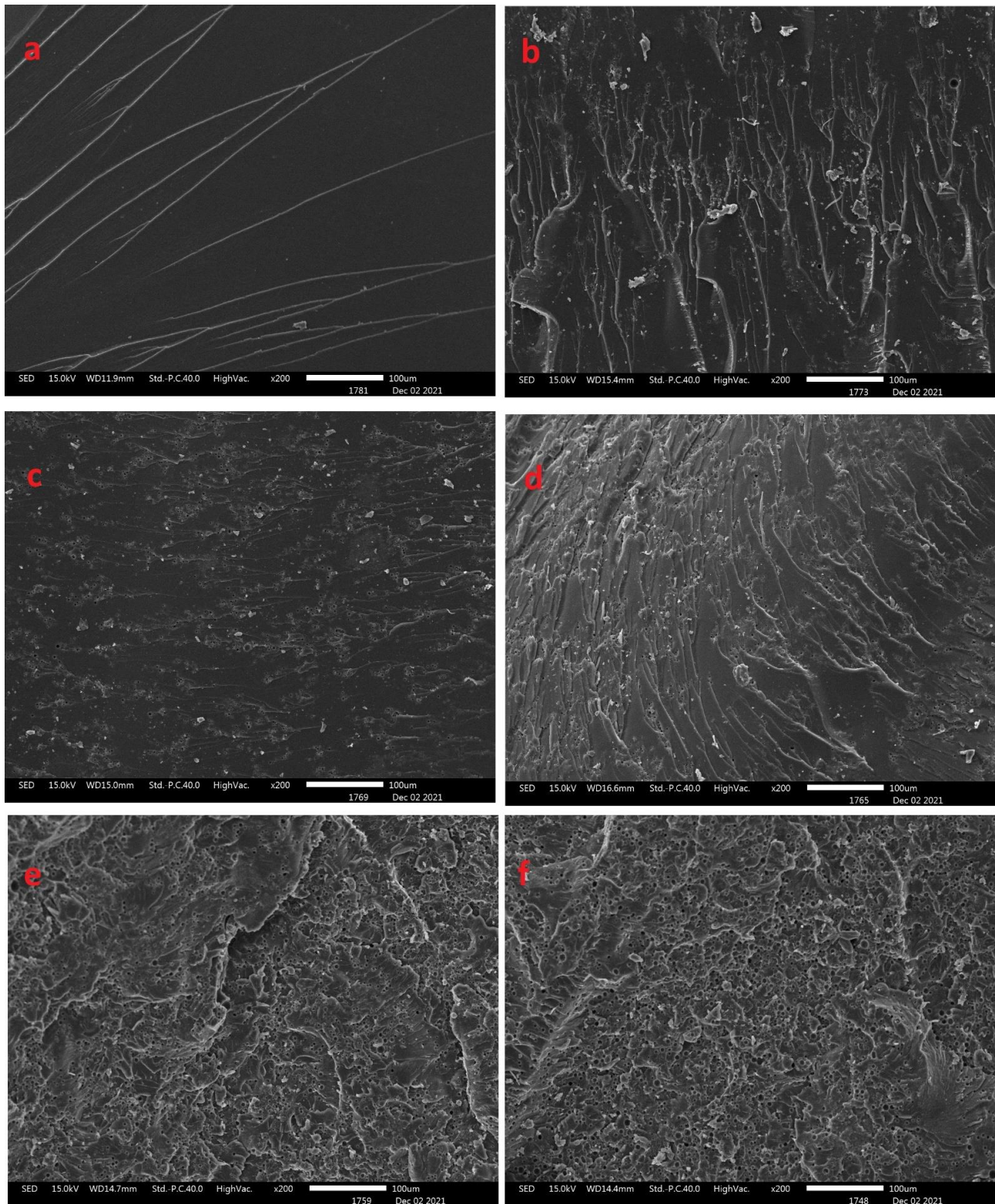


**Figure 7.** SEM micrographs of the fractured surfaces of resins: (a) neat epoxy, (b) 0.5, (c) 1.0, (d) 1.5, (e) 2.0, (f) 2.5 wt.% AFCNT-reinforced epoxy nanocomposites.

The pristine epoxy resin (Figure 7a) morphology shows linear sparse and parallel strip-like river-lines in the direction of crack propagation, confirming the brittle fracture characteristics of the epoxy resins [38]. After the addition of the functionalized AFCNTs in the matrix, the cross-sectional morphology of the material greatly changed, showing some characteristics of ductile fracture. Up to a 1.0 wt.% AFCNT content, the density of linear fringes increased and became discontinuous with the increase in AFCNT content. The change in the cross-section pattern morphology reflects that the functionalized CNTs had an effect on the crack-tip propagation path during the fracture process of the composite specimen. Thus, the energy of crack propagation was lost, and the fracture toughness of the nanocomposites was improved by increasing the energy required to achieve a continuous expansion [39].

With a 1.5 wt.% or more of AFCNT reinforcement, the change of the cross-sectional pattern was more obvious (Figure 7d–f); it was no longer parallel and straight, but was replaced by a lot of dimples, which were similar to fish scales. Moreover, a lot of stress whitening appeared at the edges of the dimples, showing better toughness. The reason for this is that PDMS molecules can be grafted onto the surfaces of the functionalized CNTs, which are compatible with the epoxy, and can also take part in the curing reaction of the matrix, thus producing good adhesion with the epoxy matrix. The energy required to destroy the interface is greatly increased, and the morphology of the interface is very different [40]. In addition, no agglomeration of CNTs were observed in any cross sections, which again proved that the dispersion of CNTs in the matrix was good. The tube structures of the stripped or pulled-out CNTs were also not observed on the cross section, indicating that the functional CNTs were completely wrapped by the epoxy, and the interface force between the CNTs and epoxy was very strong.

#### 4. Conclusions

In this work, the CNT surface was functionalized by aminopropyl-terminated polydimethylsiloxane. Functionalization was confirmed by using FTIR and SEM techniques.

The DSC results revealed that the functionalized CNTs can accelerate the curing reaction of epoxy due to the effects of  $-NH_2$  on the AFCNTs. The AFCNTs were reinforced in the epoxy resin to produce the nanocomposites, and those were systematically investigated. The prepared nanocomposites showed significant improvements in mechanical properties and temperature resistance due to the effectively improved compatibility of AFCNT with the epoxy resin. The AFCNT-reinforced nanocomposites showed gradual enhancements in the  $T_g$  as the loading was raised from 0 to 2.5 wt.%. The TGA results demonstrated that the AFCNT reinforcement significantly improved the temperature resistance of the epoxy resin and increased its thermal stability. SEM proved that the modified AFCNTs were more easily dispersed, and there was a stronger interfacial interaction between the nanofiller and matrix. The excellent mechanical properties and thermal stability of the nanocomposites confirmed that the surface modification method can be used to develop high-performance polymer materials.

**Author Contributions:** Conceptualization, Y.S. and D.Z.; methodology, Y.S. and D.Z.; software, Y.S. and D.Z.; validation, Y.S. and D.Z.; formal analysis, X.Z.; investigation, Y.S.; resources, D.Z.; data curation, Y.S.; writing—original draft preparation, Y.S. and X.Z.; writing—review and editing, D.Z.; visualization, X.Z.; supervision, D.Z.; project administration, D.Z.; funding acquisition, D.Z. All authors have read and agreed to the published version of the manuscript.

**Funding:** The work was supported by Harbin Scientific and Technological Special Fund for Innovative Talents (Grant Number 2012RFXXG093).

**Institutional Review Board Statement:** Not applicable.

**Data Availability Statement:** Not applicable.

**Conflicts of Interest:** The author(s) declared no potential conflicts of interest with respect to the research, authorship, and/or publication of this article.

## References

1. Baig, M.M.A.; Samad, M.A. Epoxy\Epoxy Composite\Epoxy Hybrid Composite Coatings for Tribological Applications-A Review. *Polymers* **2021**, *13*, 179. [[CrossRef](#)] [[PubMed](#)]
2. Jia, Z.; Feng, X.; Zou, Y. Graphene Reinforced Epoxy Adhesive For Fracture Resistance. *Compos. Part B Eng.* **2018**, *155*, 457–462. [[CrossRef](#)]
3. Zhou, H.; Fan, X.; Liu, C.; Qu, C.; Yuan, Z.; Jing, J.; Tang, Y.; Zhao, D.; Xiao, W.; Su, K. Properties of high-temperature epoxy/DDS resin systems for bonding application. *High Perform. Polym.* **2019**, *32*, 559–568. [[CrossRef](#)]
4. Zhang, J.; Liu, B.; Zhou, Y.; Essawy, H.; Chen, Q.; Zhou, X.; Du, G. Preparation of a starch-based adhesive cross-linked with furfural, furfuryl alcohol and epoxy resin. *Int. J. Adhes. Adhes.* **2021**, *110*, 102958. [[CrossRef](#)]
5. Sreehari, H.; Sethulekshmi, A.S.; Saritha, A. Bio Epoxy Coatings: An Emergent Green Anticorrosive Coating for the Future. *Macromol. Mater. Eng.* **2022**, *307*, 2200004. [[CrossRef](#)]
6. Ramón-Rez-Palma, M.T.; Hernández-Padrón, G.; Gómez, J.M.; Rojas-González, F.; Castaño, V.M. Nanostructured Epoxy-Based Anticorrosive Coatings. *Surf. Rev. Lett.* **2020**, *27*, 1950202. [[CrossRef](#)]
7. Visakh, P.M.; Nazarenko, O.B.; Sarath Chandran, C.; Melnikova, T.V.; Nazarenko, S.Y.; Kim, J.C. Effect of electron beam irradiation on thermal and mechanical properties of aluminum based epoxy composites. *Radiat. Phys. Chem.* **2017**, *136*, 17–22. [[CrossRef](#)]
8. Saif, M.J.; Naveed, M.; Zia, K.M.; Asif, M. Pristine and  $\gamma$ -irradiated halloysite reinforced epoxy nanocomposites—Insight study. *Radiat. Phys. Chem.* **2016**, *127*, 115–121. [[CrossRef](#)]
9. Rahman, M.M.; Akhtarul Islam, M. Application of epoxy resins in building materials: Progress and prospects. *Polym. Bull.* **2021**, *79*, 1949–1975. [[CrossRef](#)]
10. Shahapurkar, K.; Chavan, V.B.; Doddamani, M.; Kumar, G.C.M. Influence of surface modification on wear behavior of fly ash cenosphere/epoxy syntactic foam. *Wear* **2018**, *414–415*, 327–340. [[CrossRef](#)]
11. Zhang, K.; Wang, F.; Liang, W.; Wang, Z.; Duan, Z.; Yang, B. Thermal and Mechanical Properties of Bamboo Fiber Reinforced Epoxy Composites. *Polymers* **2018**, *10*, 608. [[CrossRef](#)]
12. Ogbonna, V.E.; Popoola, A.P.I.; Popoola, O.M.; Adeosun, S.O. A review on corrosion, mechanical, and electrical properties of glass fiber-reinforced epoxy composites for high-voltage insulator core rod applications: Challenges and recommendations. *Polym. Bull.* **2021**, *79*, 6857–6884. [[CrossRef](#)]
13. Kulik, A.J.; Kis, A.; Lukic, B.; Lee, K.; Forró, L. Mechanical Properties of Carbon Nanotubes. In *Fundamentals of Friction and Wear*; Gnecco, E., Meyer, E., Eds.; Springer: Berlin/Heidelberg, Germany, 2007; pp. 583–600. [[CrossRef](#)]
14. Gojny, F.H.; Nastalczyk, J.; Roslaniec, Z.; Schulte, K. Surface modified multi-walled carbon nanotubes in CNT/epoxy-composites. *Chem. Phys. Lett.* **2003**, *370*, 820–824. [[CrossRef](#)]
15. Bian, L.; Gao, M. Nanomechanics model for properties of carbon nanotubes under a thermal environment. *Acta Mech.* **2018**, *229*, 4521–4538. [[CrossRef](#)]
16. Niu, M.; Cui, C.; Tian, R.; Zhao, Y.; Miao, L.; Hao, W.; Li, J.; Sui, C.; He, X.; Wang, C. Mechanical and thermal properties of carbon nanotubes in carbon nanotube fibers under tension-torsion loading. *RSC Adv.* **2022**, *12*, 30085–30093. [[CrossRef](#)] [[PubMed](#)]
17. Wang, J.N.; Luo, X.G.; Wu, T.; Chen, Y. High-strength carbon nanotube fibre-like ribbon with high ductility and high electrical conductivity. *Nat. Commun.* **2014**, *5*, 3848. [[CrossRef](#)] [[PubMed](#)]
18. Li, S.; Ci, Y.; Zhang, D.; Zhang, C.; He, Y. Free arc liquid-phase dispersion method for the preparation of carbon nanotube dispersion. *Carbon Lett.* **2020**, *31*, 287–295. [[CrossRef](#)]
19. Chen, M.; Fan, G.; Tan, Z.; Yuan, C.; Xiong, D.; Guo, Q.; Su, Y.; Naito, M.; Li, Z. Tailoring and characterization of carbon nanotube dispersity in CNT/6061Al composites. *Mater. Sci. Eng. A* **2019**, *757*, 172–181. [[CrossRef](#)]
20. Mallakpour, S.; Soltanian, S. Surface functionalization of carbon nanotubes: Fabrication and applications. *RSC Adv.* **2016**, *6*, 109916–109935. [[CrossRef](#)]
21. Gojny, F.H.; Schulte, K. Functionalisation effect on the thermo-mechanical behaviour of multi-wall carbon nanotube/epoxy-composites. *Compos. Sci. Technol.* **2004**, *64*, 2303–2308. [[CrossRef](#)]
22. Setaro, A. Advanced carbon nanotubes functionalization. *J. Phys. Condens. Matter* **2017**, *29*, 423003. [[CrossRef](#)]
23. Mallakpour, S.; Soltanian, S. A facile approach towards functionalization of MWCNTs with vitamin B2 for reinforcing of biodegradable and chiral poly(ester-imide) having L-phenylalanine linkages: Morphological and thermal investigations. *J. Polym. Res.* **2015**, *22*, 183. [[CrossRef](#)]
24. Mallakpour, S.; Zadehnazari, A. The production of functionalized multiwall carbon nanotube/amino acid-based poly(amide-imide) composites containing a pendant dopamine moiety. *Carbon* **2013**, *56*, 27–37. [[CrossRef](#)]
25. Ling, X.; Wei, Y.; Zou, L.; Xu, S. Functionalization and dispersion of multiwalled carbon nanotubes modified with poly-L-lysine. *Colloids Surf. A Physicochem. Eng. Asp.* **2014**, *443*, 19–26. [[CrossRef](#)]
26. Donchak, V.; Stetsyshyn, Y.; Bratychak, M.; Broza, G.; Harhay, K.; Stepina, N.; Kostenko, M.; Voronov, S. Nanoarchitectonics at surfaces using multifunctional initiators of surface-initiated radical polymerization for fabrication of the nanocomposites. *Appl. Surf. Sci. Adv.* **2021**, *5*, 100104. [[CrossRef](#)]
27. Chen, Q.; Du, S.; Jiang, Z.; Liu, Y.; Du, R.; Zhao, G. Mechanical properties of foam sandwich with chopped-glass-fiber/carbon nanotube reinforced hierarchical structure interlayer. *Polym. Compos.* **2020**, *41*, 3411–3420. [[CrossRef](#)]
28. Farghali, A.A.; Abdel Tawab, H.A.; Abdel Moaty, S.A.; Khaled, R. Functionalization of acidified multi-walled carbon nanotubes for removal of heavy metals in aqueous solutions. *J. Nanostruct. Chem.* **2017**, *7*, 101–111. [[CrossRef](#)]

29. Fedorovskaya, E.O.; Bulusheva, L.G.; Kurenaya, A.G.; Asanov, I.P.; Okotrub, A.V. Effect of oxidative treatment on the electrochemical properties of aligned multi-walled carbon nanotubes. *Russ. J. Electrochem.* **2016**, *52*, 441–448. [[CrossRef](#)]
30. Diekmann, A.; Omelan, M.C.V.; Giese, U. Influence of Carbon Nanotube-Pretreatment on the Properties of Polydimethylsiloxane/Carbon Nanotube-Nanocomposites. *Polymers* **2021**, *13*, 1355. [[CrossRef](#)]
31. Cheng, J.X.; Cai, W.A.; Wang, Z.C.; Dayo, A.Q.; Yuan, Z.G.; Liu, W.B.; Wang, J.; Pan, Z.C. Synthesis of a novel boron-containing hyperbranched benzoxazine and its flame-retardant properties in copolymer with epoxy resin. *Polym. Adv. Technol.* **2023**, *34*, 2694–2706. [[CrossRef](#)]
32. Xu, Y.-L.; Dayo, A.Q.; Wang, J.; Wang, A.-R.; Lv, D.; Zegaoui, A.; Derradji, M.; Liu, W.-B. Mechanical and thermal properties of a room temperature curing epoxy resin and related hemp fibers reinforced composites using a novel in-situ generated curing agent. *Mater. Chem. Phys.* **2018**, *203*, 293–301. [[CrossRef](#)]
33. Rahmanian, S.; Suraya, A.R.; Roshanravan, B.; Othman, R.N.; Nasser, A.H.; Zahari, R.; Zainudin, E.S. The influence of multiscale fillers on the rheological and mechanical properties of carbon-nanotube–silica-reinforced epoxy composite. *Mater. Des.* **2015**, *88*, 227–235. [[CrossRef](#)]
34. Feng, A.; Jia, Z.; Yu, Q.; Zhang, H.; Wu, G. Preparation and characterization of carbon nanotubes/carbon fiber/phenolic composites on mechanical and thermal conductivity properties. *Nano* **2018**, *13*, 1850037. [[CrossRef](#)]
35. Ilyin, S.O.; Kotomin, S.V. Effect of Nanoparticles and Their Anisometry on Adhesion and Strength in Hybrid Carbon-Fiber-Reinforced Epoxy Nanocomposites. *J. Compos. Sci.* **2023**, *7*, 147. [[CrossRef](#)]
36. Derradji, M.; Song, X.; Dayo, A.Q.; Wang, J.; Liu, W.-B. Highly filled boron nitride-phthalonitrile nanocomposites for exigent thermally conductive applications. *Appl. Therm. Eng.* **2017**, *115*, 630–636. [[CrossRef](#)]
37. Lin, S.C.; Pearce, E.M. Epoxy resins II. The preparation, characterization, and curing of epoxy resins and their copolymers. *J. Polym. Sci. Polym. Chem. Ed.* **1979**, *17*, 3095–3119. [[CrossRef](#)]
38. Shah, A.H.; Li, X.; Xu, X.; Dayo, A.Q.; Liu, W.-B.; Bai, J.; Wang, J. Evaluation of mechanical and thermal properties of modified epoxy resin by using acacia catechu particles. *Mater. Chem. Phys.* **2019**, *225*, 239–246. [[CrossRef](#)]
39. Yuan, Z.G.; Al Hassan, M.; Wang, Z.C.; Wang, J.Y.; Wang, J.; Derradji, M.; Liu, W.B. Curing behavior, mechanical and thermal properties of epoxy-CeO<sub>2</sub> nanocomposites. *J. Appl. Polym. Sci.* **2021**, *139*, 51529. [[CrossRef](#)]
40. Ali, A.; Sohaimi, R.M.; Ismail, A.H.M. Mechanical and Fracture Surface Analysis of Higher Viscous Epoxy/Multiwalled Carbon Nanotube Nanocomposites Subjected to Flexural Loading. In *Natural and Artificial Fiber-Reinforced Composites as Renewable Sources*; Günay, E., Ed.; Intech Open: London, UK, 2018; pp. 77–86. [[CrossRef](#)]

**Disclaimer/Publisher’s Note:** The statements, opinions and data contained in all publications are solely those of the individual author(s) and contributor(s) and not of MDPI and/or the editor(s). MDPI and/or the editor(s) disclaim responsibility for any injury to people or property resulting from any ideas, methods, instructions or products referred to in the content.